

Two-Stage Multi-static Passive SAR Imaging with Reduced Complexity

Xinhua Mao

Department of Electronic Engineering
Nanjing University of Aeronautics and Astronautics
Nanjing, China
Email: xinhua@nuaa.edu.cn

Yimin D. Zhang, Moeness G. Amin

Center for Advanced communications
Villanova University
Villanova, PA 19085, USA
Email: {yimin.zhang, moeness.amin}@villanova.edu

Abstract — In this paper, a two-stage image formation approach, which combines the Fourier and sparsity-based reconstruction strategies, is proposed to effectively process the multi-static synthetic aperture radar (SAR) data. This method exploits the block sparsity of the Fourier sampling patterns which contain a number of generally disjoint subbands in the two-dimensional spatial frequency domain. The Nyquist criterion is satisfied within each subband, whereas different subbands are sparsely distributed. In the proposed approach, the Fourier-based technique is first applied to produce coarse resolution images, which are then combined to produce a high-resolution image through the exploitation of sparse reconstruction techniques. The proposed approach yields significant improvement of the resulting SAR image over Fourier-based techniques, and offers substantial reduction of the computational complexity when compared to direct sparse reconstruction. The exploitation of block sparsity-based techniques also permits practical treatment of the angle-dependency of the scattering characteristics in SAR image construction.

I. INTRODUCTION

In the literature, there are two types of algorithms that produce synthetic aperture radar (SAR) images from Fourier samples. One is based on classical linear reconstruction techniques, such as backprojection [1-2] and direct Fourier reconstruction [3-4]. These algorithms are scene-independent and, therefore, widely used in practical applications due to their simplicity. These algorithms, however, require that the data are sampled at the Nyquist rate. When the data are under-sampled or otherwise missing samples are present, linear reconstruction techniques may result in performance degradation, such as the appearance of undesired artifacts. To solve this problem, nonlinear reconstruction techniques, particularly the sparse reconstruction or compressive sensing approaches, have been found useful in recent years [5-6]. Sparse reconstruction methods can accurately reconstruct sparse scenes with a small number of randomly sampled Fourier samples.

Passive radars suffer from low signal bandwidths and low carrier frequencies [7]. As such, it is important to exploit multiple available illuminators for multi-static operation. In this paper, we propose an effective multi-static passive SAR

imaging method using a two-stage approach in which the Fourier-based and sparsity-based signal reconstruction strategies are subsequently applied. The multi-static radar being considered consists of multiple stationary illuminators and a single moving receiver, but the extension to multiple receivers is straightforward. In each subband of Fourier samples that correspond to a bistatic illuminator/receiver pair, the sampling satisfies the Nyquist criterion. As such, a Fourier-based reconstruction method is first applied to each subband, which corresponds to a bistatic pair, to produce a coarse-resolution image. These images are then combined across all the subbands to produce a high-resolution image through the exploitation of sparse reconstruction techniques. The mapping between the coarse-resolution Fourier-based images and the fused high-resolution image in this stage allows us to partition the entire image to multiple sub-images and process them separately. Thus, the required complexity is significantly reduced as compared to the direct reconstruction of the entire image at the same time. On the other hand, when compared with Fourier-based techniques, the proposed approach avoids the artifact effect due to disjoint and sparse observation subbands. In addition, the exploitation of block sparsity-based techniques enables practical treatment of the angle-dependency of the scattering characteristics in SAR image construction.

II. MULTI-STATIC PASSIVE SAR

In this section, we first introduce the tomographic interpretation for a bistatic passive radar pair, and then extend the model to a multi-static radar case.

A. Bi-static Radar

Consider a bistatic radar geometry as shown in Fig. 1(a). We assume the 2-D geometry without loss of generality, but the results can be easily extended to the 3-D case. In our geometry, the center of the interested scene is defined as the origin of coordinate system, whereas the positions of the transmitter and the receiver are determined by their polar radius and polar angle pairs, respectively denoted as $[r_{\text{Tc}}, \theta_{\text{T}}]$ and $[r_{\text{Rc}}, \theta_{\text{R}}]$. We assume that an arbitrary point target, located at (x_t, y_t) , with a scattering coefficient is σ . The ranges from the transmitter and receiver to the target are denoted by r_{T} and r_{R} , respectively.

The work of X. Mao is supported in part by the National Nature Science Foundation of China (Grant No. 61301210) and Nature Science Foundation of Jiangsu Province (Grant No. BK20130815).

The transmitter emits signal $s(\tau) = \exp(i2\pi f\tau)$ to illuminate the service area. After demodulation, the received signal can be expressed as

$$r(\tau) = \sigma \cdot \exp\left[-i2\pi f \frac{r_T + r_R}{c}\right], \quad (1)$$

After motion compensation to the scene center, it becomes

$$\hat{r}(\tau) = \sigma \cdot \exp\left[i2\pi f \frac{r_{Tc} + r_{Rc} - r_T - r_R}{c}\right]. \quad (2)$$

Under the plane wavefront assumption, it can be rewritten as

$$\begin{aligned} \hat{r}(\tau) &= \sigma \cdot \exp\left\{i \frac{2\pi f}{c} [x_t (\cos \theta_T + \cos \theta_R) + y_t (\sin \theta_T + \sin \theta_R)]\right\} \\ &= \sigma \cdot \exp\left\{i (x_t k_x + y_t k_y)\right\}, \end{aligned} \quad (3)$$

where

$$k_x = \frac{2\pi f}{c} (\cos \theta_T + \cos \theta_R) \quad \text{and} \quad k_y = \frac{2\pi f}{c} (\sin \theta_T + \sin \theta_R) \quad (4)$$

are the spatial frequencies in the x and y directions, respectively. They can also be conveniently expressed in the polar format as:

$$\begin{aligned} k_r &= \sqrt{k_x^2 + k_y^2} = \frac{4\pi f}{c} \cos\left(\frac{\theta_T - \theta_R}{2}\right), \\ \theta_b &= \text{atan}\left(\frac{k_y}{k_x}\right) = \text{atan}\left(\frac{\sin \theta_T + \sin \theta_R}{\cos \theta_T + \cos \theta_R}\right) = \frac{\theta_T + \theta_R}{2}. \end{aligned} \quad (5)$$

From (3), it is clear that the data after preprocessing, i.e., $\hat{r}(\tau)$, is essentially a sample of the target in the spatial frequency (wavenumber) domain. The sample position is determined by the azimuth angles of the transmitter/receiver and the frequency of the transmitted signal. As illustrated in Fig. 1(b), for a single-frequency signal, the azimuth angle of the transmitter and the signal frequency respectively determine the position and size of the red circle, whereas the bisection that divides the azimuth angles of the transmitter and receiver determines the sample direction, shown as the dashed line. The sample position is the intersection of the red circle and the dashed line.

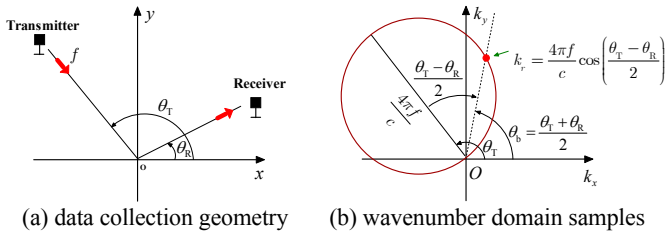


Fig. 1. Data collection geometry and wavenumber domain samples for a bistatic transmitter/receiver pair.

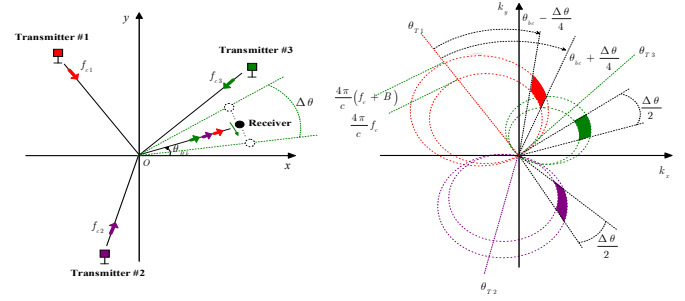
B. Multi-static Passive SAR

Now we consider the signal model in a multi-static case with J illuminators, where the j th illuminator transmits a signal with bandwidth B_j and a distinct carrier frequency f_{c_j} . The receiver receives the scattered echo from the scene at a constant repeat time interval. During the coherent processing interval (CPI) corresponding to an accumulated angle $\Delta\theta$, it collects K sample series at K different azimuth positions. Each series contains the scene echo corresponding to the J

illuminators. From (3), we obtain the signal model for the multi-static SAR as

$$\begin{aligned} r(j, k, l) &= \sigma \cdot \exp\left\{i \frac{2\pi(f_{c_j} + f_l)}{c} [x_t (\cos \theta_{T_j} + \cos \theta_{R_k}) + y_t (\sin \theta_{T_j} + \sin \theta_{R_k})]\right\} \\ &= \sigma \cdot \exp\left\{i [x_t k_x^{jkl} + y_t k_y^{jkl}]\right\}. \end{aligned} \quad (6)$$

Due to space and frequency diversity, i.e., the variation of f_{c_j} , f_l , θ_{T_j} , and θ_{R_k} , the data collected by the airborne multi-static SAR represent multiple samples in the spatial frequency domain. Typically, the samples in f_l and θ_{R_k} are dense and satisfy the Nyquist requirement, whereas the samples in f_{c_j} and θ_{T_j} are often sparse. Therefore, the sample support is usually block sparse in the wavenumber domain. For the multi-static passive radar configuration shown in Fig. 2(a), the corresponding sample support pattern is depicted in Fig. 2(b).



(a) radar geometry (b) wavenumber domain sample pattern

Fig. 2. Wavenumber domain support pattern for multi-static SAR.

III. IMAGE FORMATION

For the multi-static passive radar, as discussed in the previous section, the wavenumber domain sample patterns are block sparse, i.e., the observed support areas are composed of a number of sparsely distributed subbands. In each subband, the data are sampled at Nyquist rate. Considering this specific sample pattern, we propose an effective two-stage image formation algorithm, which combines the linear and nonlinear reconstruction techniques. In the first-stage, a series of coarse-resolution images are individually formed from the subband data by using a linear reconstruction algorithm, since the subband data are intensively sampled. In the second stage, the information extracted from the coarse-resolution images is exploited by a sparse reconstruction technique to form an image with a finer resolution. This two-stage processing strategy is illustrated in Fig. 3.

A. First-Stage Image Formation

The observed subband samples are, in general, uniformly spaced in the polar (f_l, θ_{R_k}) domain. As such, they become non-uniformly spaced after being mapped to the Cartesian spatial frequency domain (k_x, k_y) . Therefore, to exploit available computationally efficient algorithms, such as the fast Fourier transform (FFT), a 2-D interpolation of the sampled data onto a rectangular grid in the (k_x, k_y) domain is performed.

After performing polar format transformation, the signal in (6) can be expressed as

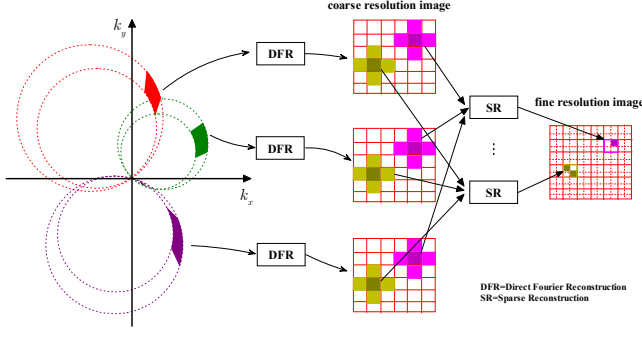


Fig. 3 Illustration of the proposed two-stage image formation method

$$r(j, k, l) = \sigma \cdot \exp\{i[x_l k_x^k + y_l k_y^l]\}, \quad (8)$$

where $k_x^k = k_x^j + \left(k - \frac{K}{2}\right)\Delta_{k_x}$, $k=1, \dots, K$, and $k_y^l = k_y^j + \left(l - \frac{L}{2}\right)\Delta_{k_y}$, $l=1, \dots, L$, are the resampled positions in the k_x and k_y domains, respectively. For the j th subband, the support center of wavenumber domain is set as

$$k_{xc}^j = \frac{2\pi f_{cj}}{c} (\cos \theta_{Tj} + \cos \theta_{Rc}), \quad k_{yc}^j = \frac{2\pi f_{cj}}{c} (\sin \theta_{Tj} + \sin \theta_{Rc}). \quad (9)$$

Performing 2-D FFT on (8) with respect to k and l yields a series of coarse-resolution images, expressed as

$$r(j, n, m) = \sigma \cdot A^j \left(\frac{n}{K\Delta_{k_x}} - x_t, \frac{m}{L\Delta_{k_y}} - y_t \right) \cdot \exp\{i[x_t k_{xc}^j + y_t k_{yc}^j]\}, \quad (10)$$

where $A^j(x, y)$ is the point spread function for the j th subband data, whereas $1/(K\Delta_{k_x})$ and $1/(L\Delta_{k_y})$ are the pixel sizes in the x and y directions, respectively.

From (10), we can obtain a coarse estimate of target position as

$$\bar{y}_t = \frac{n_0}{K\Delta_{k_x}}, \quad \bar{y}_t = \frac{m_0}{L\Delta_{k_y}}, \quad (11)$$

whose respective accuracies are $1/(K\Delta_{k_x})$ and $1/(L\Delta_{k_y})$. In (11), n_0 and m_0 are the pixel indexes of the target location in the x and y directions, respectively.

B. Second-Stage Image Formation

Because the observation subbands are sparsely distributed in the wavenumber domain, Fourier reconstruction may not yield a desirable image resolution and low sidelobe levels. In addition, it is difficult to perform coherent Fourier reconstruction across the entire observation subbands when the scattering coefficients depend on the aspect of the illuminators.

In such situations, the recently developed nonlinear reconstruction techniques, i.e., the sparse signal reconstruction and compressive sensing approaches, can provide an effective target reconstruction capability, provided that the scene is sparse. Such sparse scene imaging problems to be considered herein are important in practice because many real-world scenes are either strictly sparse or can be approximated with a small number of strong scatterers. As such, in the sequel, we employ sparse reconstruction techniques in the second image formation stage to fuse the coarse-resolution images.

In this stage, each coarse-resolution image pixel is divided into $N \times N$ fine resolution pixels. Therefore, the size of the new pixel in the range and azimuth becomes $1/(NK\Delta_{k_x})$ and $1/(NL\Delta_{k_y})$, respectively. For the j th illuminator, the signals at the coarse-resolution cell and the fine-resolution cell can be associated by a transform matrix, expressed as

$$r^{(j)} = \Phi^{(j)} \mathbf{w}^{(j)}, \quad j=1, 2, \dots, J, \quad (12)$$

where $r^{(j)}$ is the value of the pixel generated in the coarse-resolution image, $\mathbf{w}^{(j)} = (w_1^j, \dots, w_{N^2}^j)^T$ is the fine-resolution pixel vector to be reconstructed. In addition, $\Phi^{(j)}$ is a sensing row vector of size $1 \times N^2$, whose n th element is expressed as

$$\phi_n^{(j)} = A^j(x_c - x_n, y_c - y_n) \cdot \exp\{i[x_n k_{xc}^j + y_n k_{yc}^j]\}, \quad (13)$$

where (x_c, y_c) and (x_n, y_n) are the coordinates of the coarse-resolution pixel cell and the n th fine-resolution pixel, respectively.

To fully account for the spreading effects of the image, it is desirable to exploit multiple coarse-resolution pixels to construct the fine-resolution images in the second stage. Toward this end, we modify (12) by using Q coarse-resolution pixels, yielding the following expression:

$$\tilde{r}^{(j)} = \tilde{\Phi}^{(j)} \tilde{\mathbf{w}}^{(j)}, \quad j=1, 2, \dots, J, \quad (14)$$

where $\tilde{r}^{(j)} = (r_1^j, \dots, r_Q^j)^T$ is a vector containing the values of Q selected neighboring coarse-resolution pixels, $\tilde{\mathbf{w}}^{(j)}$ represents a vector of the unknown fine-resolution pixels contained in the Q coarse-resolution pixels, and $\tilde{\Phi}^{(j)}$ is a $Q \times QN^2$ sensing matrix, whose (q, n) th element is

$$\phi_{q,n}^{(j)} = A^j(x_q - x_n, y_q - y_n) \cdot \exp\{i[x_n k_{xc}^j + y_n k_{yc}^j]\}, \quad (15)$$

with (x_q, y_q) denoting the position of the q th coarse-resolution pixel.

As we described earlier, in multi-static passive SAR, the scattering coefficients differ with respect to different illuminators due to their different aspect angles. That is, the fine-resolution pixel coefficients to be estimated, which are expressed as vectors $\tilde{\mathbf{w}}^{(j)}$ in (14), are different for different index j . Nevertheless, because it is likely that the same sparse scatterers make contribution to the observation data irrespective of the illuminators, the positions of the nonzero entries in the vectors $\tilde{\mathbf{w}}^{(j)}$ are identical or at least highly overlap. This characteristic is referred to as the block sparsity or group sparsity [8]. This type of problems can be effectively solved using techniques that take such property into account, such as block-sparsity based compressed sensing [8], multi-task compressed sensing [9-10], and distributed compressed sensing [11].

Equation (14) is solved for each coarse resolution pixel and repeated until all the coarse-resolution pixels are processed. Finally, all the obtained fine-resolution sub-images are mosaicked to obtain the high-resolution image of the entire scene. The proposed second-stage processing is illustrated in Fig. 3. Note that while the fine-resolution pixel coefficients are computed for Q coarse-resolution pixels each time, only the results obtained for the underlying coarse-resolution pixel is maintained and those belonging to the neighboring coarse-resolution pixels are discarded.

IV. EXPERIMENTAL RESULTS

Simulations are performed to verify the effectiveness of the proposed technique. Assume that the passive radar system employs 8 stationary illuminators with a moving receiver. The respective frequencies and azimuth angles of the illuminators are summarized in Table 1, whereas the bandwidth of each signal is assumed to be 20 MHz. It is assumed that, for the sparse scene consisting of a collection of point targets, as shown in Fig. 4, the receiver changes its azimuth angle from 11° to 17° during the observation period. The resulting wavenumber domain support is shown in Fig. 5. For each bistatic pair corresponding to an illuminator, the scattering coefficients are considered time-invariant because of the small azimuth angle of the receiver. The scattering coefficients, however, vary independently for bistatic pairs associated with different illuminators.

Table 1. Frequency and Azimuth Angles of the 8 Illuminators

Illuminator	1	2	3	4	5	6	7	8
f_c (MHz)	450	550	500	480	610	520	630	580
Angle($^\circ$)	5	10	45	25	30	20	15	50

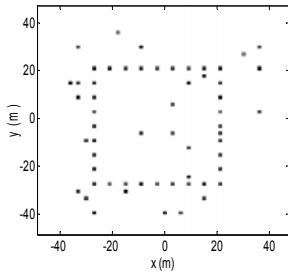


Fig. 4 Targets locations.

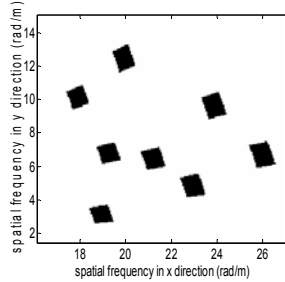


Fig. 5 Sample support area.

For comparison, the result obtained from direct Fourier-based imaging is shown in Fig. 6(a). The images obtained in the eight subbands are noncoherently combined because the scattering coefficients are aspect-dependent and, thereby, their phases cannot be coherently aligned. As we discussed earlier, the quality of the resulting image is undesirable as it suffers from a poor image resolution and high sidelobe levels. We also show the results when conventional compressive sensing techniques, which do not consider the group sparsity, are used to reconstruct the image. The image shown in Fig. 6(b) is the sum of the image magnitudes computed separately for each illuminator to account for their different scattering coefficients.

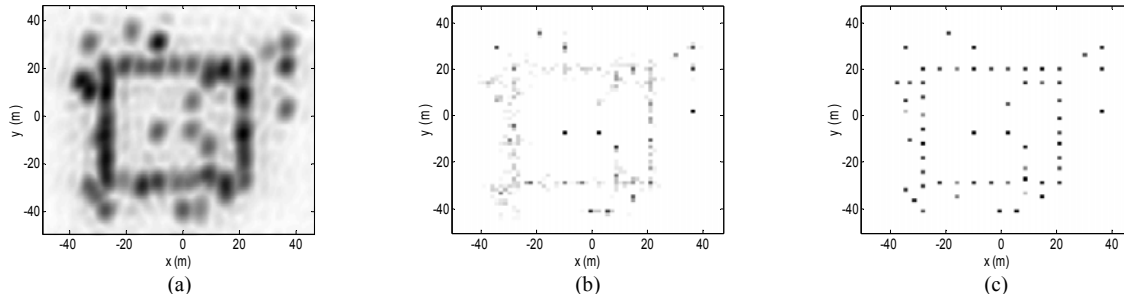


Fig. 6 Images produced by (a) Fourier-based imaging, (b) conventional compressed sensing, and (c) the proposed two-stage method.

In the proposed two-stage imaging technique, the eight coarse-resolution images, respectively obtained through the Fourier transform, are fused to form a fine-resolution image using the block orthogonal matching pursuit (BOMP) [8] technique. It is evident from Fig. 6(c) that the resulting image recovers the high-resolution pixels with a high fidelity.

V. CONCLUSION

In this paper, we have proposed an effective two-stage technique for multi-static passive SAR imaging. By combining Fourier-based approach and group sparsity based signal reconstruction methods, the proposed technique achieves high-quality SAR imaging with a low complexity.

REFERENCES

- [1] M. D. Desai and W. K. Jenkins, "Convolution backprojection image reconstruction for spotlight mode synthetic aperture radar," *IEEE Trans. Image Proc.*, vol. 1, no. 4, pp. 505-517, 1992.
- [2] V. Krishnan, J. Swoboda, C. E. Yarman, and B. Yazici, "Multistatic synthetic aperture radar image formation," *IEEE Trans. Image Proc.*, vol. 19, no. 5, pp. 1290-1306, 2010.
- [3] J. L. Walker, "Range-Doppler imaging of rotating objects," *IEEE Trans. Aerosp. Electron. Syst.*, vol. 16, pp. 15-22, 1980.
- [4] Y. Wu and D. C. Munson, "Multistatic synthetic aperture imaging of aircraft using reflected television signals," in *Proc. SPIE*, vol. 4382, Aug. 2001.
- [5] D. L. Donoho, "Compressed sensing," *IEEE Trans. Inform. Theory*, vol. 52, no. 4, pp. 1289-1306, 2006.
- [6] E. Candes, J. Romberg, and T. Tao, "Robust uncertainty principles: exact signal reconstruction from highly incomplete frequency information," *IEEE Trans. Inform. Theory*, vol. 52, no. 2, pp. 489-509, 2006.
- [7] Y. D. Zhang and B. Himed, "Moving target parameter estimation and SFN ghost rejection in multistatic passive radar," in *Proc. IEEE Radar Conf.*, Ottawa, Canada, April 2013.
- [8] C. E. Yonina, K. Partick, and B. Helmut, "Compressed sensing of block-sparse signals: uncertainty relations and efficient recovery," *IEEE Trans. Signal Proc.*, vol. 58, no. 6, pp. 3042-3054, 2010.
- [9] S. Ji, D. Dunson, and L. Carin, "Multitask compressive sensing," *IEEE Trans. Signal Proc.*, vol. 57, no. 1, pp. 92-106, 2009.
- [10] Q. Wu, Y. D. Zhang, M. G. Amin, and B. Himed, "Complex multitask Bayesian compressive sensing," in *Proc. IEEE Int. Conf. Acoustics, Speech, Signal Proc.*, Florence, Italy, May 2014.
- [11] B. Dror, B. W. Michael, F. D. Marco, S. Shriram, and G. B. Richard, "Distributed compressed sensing of jointly sparse signals," in *Proc. Asilomar Conf. Signals, Systems and Computers*, Pacific Grove, CA, pp. 1537-1541, Nov. 2005.